*J Water Environ Nanotechnol* 2026, 11(4): 535-553

10.22090/jwent.2026.2082760.2049

RESEARCH PAPER

# Response Optimization of Metformin Degradation Using Bio-Synthesized $Fe_3O_4$ Nanoparticles

***Shital Prashant Dehankar* and *Ratnadip R. Joshi****

Department of Chemical Engineering, Dr. Vishwanath Karad MIT World Peace University, Pune, Maharashtra, India

*Corresponding Author. Email: ratnadip.joshi@mitwpu.edu.in

**Article History:**

Received: 2026-01-01

Revised: 2026-03-16

Accepted: 2026-04-18

***How to cite this article***

Dehankar S P, Joshi R R. Response Optimization of Metformin Degradation Using Bio-Synthesized $Fe_3O_4$ Nanoparticles. J Water Environ Nanotechnol. 2026, 11(4): 535-553, DOI: 10.22090/jwent.2026.2082760.2049

## HIGHLIGHTS

- Neem leaf extract was used for the green synthesis of $Fe_3O_4$ nanoparticles.
- Synthesized nanoparticles were characterized using FTIR, XRD, SEM and VSM.
- Taguchi L9 design optimized four parameters for metformin degradation.
- $Fe_3O_4$ achieved 91.3% degradation and retained activity over four reuse cycles.

## ABSTRACT

**Aim:** This paper examines the green synthesis of $Fe_3O_4$ nanoparticles using neem (*Azadirachta indica*) leaf extract, the catalytic ability of the nanoparticles in the degradation of the pharmaceutical pollutant metformin, and process optimization by the Taguchi statistical design.

**Methods:** Plant-assisted precipitation was used to form $Fe_3O_4$ nanoparticles, which were analyzed by Fourier transform infrared spectroscopy (FTIR), X-ray diffraction (XRD), scanning electron microscopy (SEM), and vibrating sample magnetometry (VSM) techniques. The batch degradation experiments were carried out under various conditions of operation such as the catalyst dosage, pH of the solution, initial concentration of the metformin, and time of the reaction. A Taguchi L9 orthogonal array was used to optimize process parameters, and catalyst stability was determined by repeated reuse cycles.

**Results:** Stabilization of the magnetite formation that was stabilized by phytochemicals of neem was confirmed via FTIR and XRD. Nanoscale spherical particles with reduced morphological degradation following reuse were found in SEM. Taguchi model has shown pH to be the most significant factor, followed by optimal conditions that brought out an approximate 91% degradation. Residual analysis was used to confirm the model adequacy; the efficiency decreased slightly during four reuse cycles, that is, on the surface and not due to structural failure.

**Conclusion:** These findings indicate that neem-based $Fe_3O_4$ nanoparticles are a potent and green catalyst in removing metformin. Green synthesis and the Taguchi-based optimization give significance to this system regarding its sustainable usage in wastewater treatment.

**KEYWORDS:** *Green synthesis, $Fe_3O_4$ nanoparticles, Metformin degradation, Taguchi optimization, Catalytic reuse*

©2026 The Author(s). Published by the Iranian Environmental Mutagen Society. This work is licensed under the Creative Commons Attribution 4.0 International License (CC BY 4.0). To view a copy of this license, visit http://creativecommons.org/licenses/by/4.0/.

## 1. INTRODUCTION

### 1.1 Pharmaceuticals in Water Systems

Contamination of pharmaceuticals is the biggest environmental issue to arise in the past 20 years, especially with the growing consumption and incomplete elimination of their effects on wastewater treatment. Of these pollutants, special importance has become metformin, a commonly prescribed antidiabetic medication. Metformin is prescribed over 120 million times annually throughout the world, which leads to a great amount of environmental dispersion [1,2]. Many pharmaceuticals are metabolised, and metformin is virtually excreted, which is why it is often found in wastewater, surface water, groundwater, and even drinking water networks with treatment [1-3]. Its resilience in the water bodies also aids in developing guanylurea, a transformation product obtained through microbial processes, which is also detected in the water bodies regularly [3].

Environmental exposure to metformin and its derivatives is not the type of exposure a drug should have. The products of chlorination synthesised during any disinfection process on water have shown either toxic properties to mammals and aquatic life, such as intestinal injury in animal models and cytotoxicity in human cells [2,4]. The concentrations being identified in the environment have been associated with oxidative stress, genotoxic effects, and reproductive interference among aquatic life, including fish and invertebrates [3,5,6]. These kinds of results raise a question about the fear of possible health effects on both the ecosystems and the human population who come in contact with polluted sources of drinking water.

### 1.2 Need for Advanced Treatment

Traditional wastewater treatment facilities (WWTPs) partially take out metformin and discharge it further into natural water bodies [5,7]. This is inefficient due to the fact that WWTPs have a low capacity to degrade refractory organic compounds that undergo slow biological mineralisation [8]. Moreover, advanced oxidation processes (AOPs) and catalytic degradation strategies have gained interest as alternative methods of treatment since they have the potential to boost reaction kinetics, selectivity, and reduce by-products (P127; P128). Metallic oxide-based catalysts, magnetic nanoparticles, and supported photocatalysts are effective in degrading pharmaceuticals, overcoming the problem of chemical consumption, sludge generation, and slow biodegradation [8,9]. Nevertheless, the obstacles to implementation in industry remain because of complexity, cost, and material sustenance [10,11].

### 1.3 Green Nanotechnology

Magnetic iron oxide ($Fe_3O_4$) nanoparticles have the characteristics of high surface area, magnetic recovery, and activity, which makes them superior in catalytic water treatment [12]. Conventional synthesis pathways can be associated with the use of toxic reducing agents, harsh conditions of the reaction, and the use of high-energy, creating environmental and economic concerns [13]. Plant extracts give an environmentally friendly alternative to the green synthesis. Neem leaves (*Azadirachta indica*) have polyphenols and phytochemicals that are able to reduce iron salts and stabilise nanoparticles to form non-toxic $Fe_3O_4$ with a defined particle size and are superparamagnetic [12]. This nature-friendly strategy increases the stability of nanoparticles and their catalytic characteristics and reduces their environmental impact [13,14]. It is also in tandem with the principles of green chemistry, which compensate for the lack of sustainability in the traditional production of nanomaterials.

### 1.4 Neem Waste Valorisation Concept

Neem biomass used to produce nanoparticles is a strategy of the circular economy in which agricultural wastes can be transformed into useful functional substances. Recycling the neem waste will also help decrease the problem of biomass disposal and produce high-value nanocatalysts that may be used in the application of water treatment [15,16]. The two-fold advantage encourages resource use efficiency, a decrease in pollution, and economic incentives for green technologies.

### 1.5 Taguchi Statistical Optimisation

Taguchi design, based on orthogonal matrices, has been used in environmental engineering to optimise treatment systems. It allows recognising the significant factors of operations using the least amount of experimental runs, using fewer resources and treating as many as possible [17]. The nano-catalytic reactions, where the reactions depend on the interaction of the pH, the concentration of the pollutant (or other relevant substances), the dosage of the catalysts and reaction time, are of particular concern in terms of such statistical optimisation.

### 1.6 Research Gap

Despite the extensive research on $Fe_3O_4$ nanoparticles, there is a paucity of literature on neem-derived $Fe_3O_4$ as a catalyst in degrading persistent pharmaceuticals like metformin. Also, no systematic optimisation experiments with the Taguchi approach were used for metformin degradation, which is a gap in synthesis innovation as well as performance optimisation.

### 1.7 Objectives

Accordingly, this study aims to:

1) synthesise $Fe_3O_4$ nanoparticles using neem waste extract,
2) characterise their structure and properties,
3) assess catalytic degradation efficiency toward metformin, and
4) optimise treatment parameters using Taguchi statistical design.



*J Water Environ Nanotechnol,* 2026, 11(4): 535-553
10.22090/jwent.2026.2082760.2049

## 2. MATERIALS AND METHODS

### 2.1 Materials

Sources of iron precursors were ferric nitrate ($Fe(NO_3)_3·9H_2O$) and ferric sulfate ($FeSO_4·7H_2O$). These metal salts were used as the main reactants for the $Fe_3O_4$ nanoparticle. To make a reducing and capping agent, fresh neem (*Azadirachta indica*) leaves were obtained locally to form a plant extract used as the reducing and capping agent. Stock solutions for degradation experiments were prepared using metformin hydrochloride of pharmaceutical grade. Other reagents were sodium hydroxide (NaOH) and ammonium hydroxide ($NH_4OH$) to check the pH, ethanol and distilled water to wash the solution, and hydrochloric acid (HCl) to adjust the solution to the required pH. The chemicals were not further purified. Table 1 presents a summary of materials used, purities, suppliers, and purposes.

### 2.2 Synthesis of $Fe_3O_4$ Nanoparticles via Green Route

The green synthesis method was selected to produce $Fe_3O_4$ nanoparticles with neem leaf extract, a bioreducing and stabilising solution. The synthetic pathway was made up of the formation of precursor solutions, the preparation of extracts, precipitation of nanoparticles, separation, and subsequent treatment (Fig. 1).

The aqueous precursor solutions were made by dissolving the $Fe(NO_3)_3$ and $FeSO_4$ in 100 mL of distilled water under constant magnetic stirring. The stoichiometric molar ratio of the salts in the mixture, 2:1 ($Fe^{3+}$: $Fe^{2+}$), is consistent with the formation of magnetites under the same conditions. Heat was applied to the mixture to 60–80 °C in order to create homogeneous mixing and begin reaction conditions. The mass of precursors was calculated depending on the hydration state of the compound, as represented in the synthesis document, in which measured masses were 3.49 g $Fe(NO_3)_3·9H_2O$ and 1.20 g $FeSO_4·7H_2O$ in the reaction system. Precursor mass ratios and reaction stoichiometry are given in Table 2.

The extract of neem was made by boiling the washed leaves of neem in distilled water for 15- 30 minutes until the bioactive compounds were extracted. The extract was filtered to facilitate the removal of solids from the plant and left to cool, after which it was stored to be eventually used as the reducing agent. Phytochemicals found (polyphenols and flavonoids) are reducing and stabilising agents, and they facilitate the nucleation of nanoparticles.

Constant stirring was applied to the hot iron precursor solution, and the neem extract was added drop by drop. An increase in the colour of the reduction of $Fe^{3+}$ and $Fe^{2+}$ was noticed, and the formation of $Fe_3O_4$ nanoparticles was assisted by the gradual increase of the pH with the help of NaOH or $NH_4OH$. The mixture was stirred by incubating at 80 °C for another hour to stabilise the particles.

To isolate the nanoparticles, the black precipitate was cooled and centrifuged at 3000-5000 rpm for 10 minutes, ensuring

**Table 1:** Materials Used

| Material | Grade/Purity | Supplier | Purpose |
|---|---|---|---|
| Ferric nitrate ($Fe(NO_3)_3·9H_2O$) | Analytical | Sigma-Aldrich / Merck | $Fe^{3+}$ precursor |
| Ferrous sulfate ($FeSO_4·7H_2O$) | Analytical | Sigma-Aldrich / Merck | $Fe^{2+}$ precursor |
| Neem leaves (Azadirachta indica) | Fresh biological | Local source | Extract for green reduction/ capping |
| Sodium hydroxide (NaOH) | Analytical | Merck | pH adjustment/precipitation |
| Ammonium hydroxide ($NH_4OH$) | Analytical | Loba Chemie | pH regulation |
| Ethanol | Analytical | Merck | Washing nanoparticles |
| Distilled water | Laboratory purity | In-house | Solvent |
| Metformin hydrochloride | Pharmaceutical grade | TCI / Sigma | Pollutant stock preparation |
| Hydrochloric acid (HCl) | Analytical | Merck | pH adjustment |

**Table 2:** Precursor quantities and stoichiometric ratio used for $Fe_3O_4$ nanoparticle synthesis

| Component | Chemical formula | Molecular weight (g/mol) | Moles used (mmol) | Mass added (g) | Function |
|---|---|---|---|---|---|
| Ferric nitrate | $Fe(NO_3)_3·9H_2O$ | 404 | 8.64 | 3.49 | $Fe^{3+}$ ion source |
| Ferrous sulfate | $FeSO_4·7H_2O$ | 278 | 4.32 | 1.20 | $Fe^{2+}$ ion source |
| Neem extract | Aqueous extract | — | Excess | 10–30 mL | Reducing/stabilising agent |
| NaOH / $NH_4OH$ | — | — | Adjusted | As required | Precipitating agent |

(Notes: $Fe^{3+}$:$Fe^{2+}$ molar ratio maintained at 2:1.)

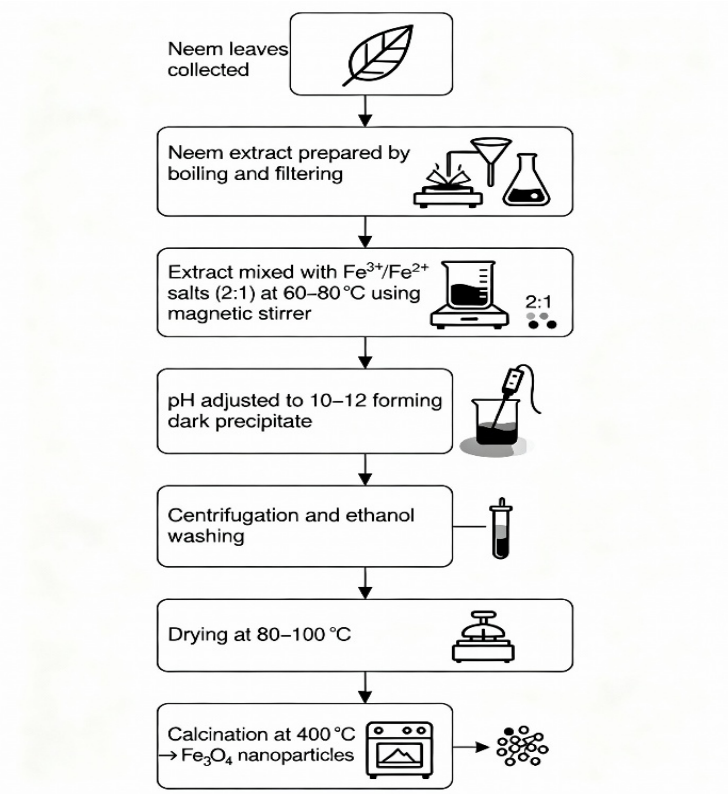



**Fig. 1**: Schematic representation of the green synthesis of $Fe_3O_4$ nanoparticles using neem extract, showing extract preparation, precursor mixing, reduction–precipitation, separation, drying, and calcination steps.

**Table 3:** Instruments used for nanoparticle characterisation

| Instrument | Model/Manufacturer | Measurement role |
|---|---|---|
| X-ray diffractometer (XRD) | PANalytical / Bruker D8 Advance | Crystal phase identification |
| FTIR spectrometer | Jasco / PerkinElmer Spectrum-Two | Functional group confirmation |
| Scanning electron microscope (SEM) | JEOL JSM series / FEI Nova NanoSEM | Morphology analysis |
| Vibrating sample magnetometer (VSM) | Lakeshore / Quantum Design | Magnetic property analysis |
| UV-Vis spectrophotometer | Shimadzu UV-1800 / Agilent Cary 60 | Metformin concentration analysis |

that the nanoparticles and the solution separated. Washing was done (3-5 times) with distilled water and ethanol to wash off chloride ions, unreacted precursors, and biomolecular remnants. Overnight, the washed powder was dried in a hot-air oven at 80–100 °C. To enhance crystallinity, calcination at 400 °C and 4 hours was carried out (Fig. 1).

### 2.3 Characterisation Techniques

Synthesised nanoparticles of $Fe_3O_4$ were obtained by subjecting them to physicochemical characterisation employing advanced analytical instruments listed in Table 3.

- The identification of the crystal phase and the formation of $Fe_3O_4$ were confirmed by the use of X-ray diffraction (XRD).
- The presence of functional groups on neem extracts was found using Fourier transform infrared spectroscopy FTIR which is related to Fe-O vibration and biomolecule capping.
- Morphological and particle size distribution data were obtained through the use of scanning electron microscopy (SEM)
- VSM was used to assess magnetic properties that were of relevance in the separation and recovery of catalysts.



*J Water Environ Nanotechnol,* 2026, 11(4): 535-553
10.22090/jwent.2026.2082760.2049

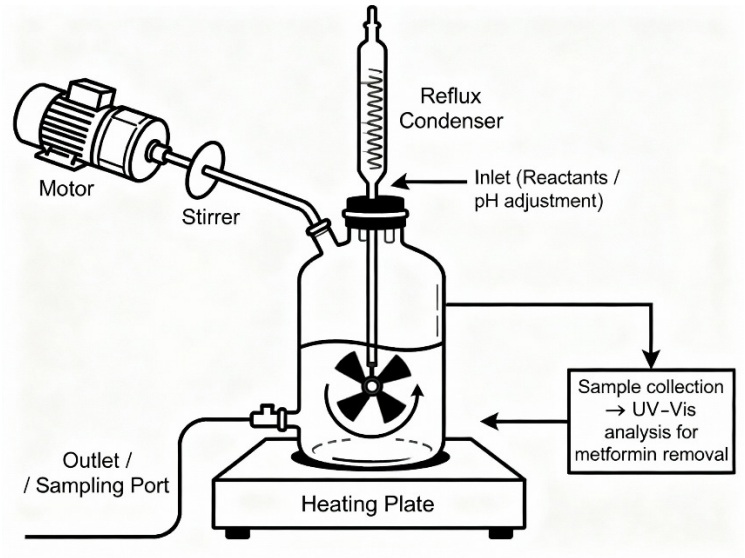



**Fig. 2**: Schematic illustration of the batch reactor setup used for metformin degradation experiments, showing reflux condenser, mechanical stirring, heating plate, inlet for reagent addition, and outlet for sampling and analysis.

**Table 4:** Taguchi orthogonal array matrix for degradation experiment

| Trial | pH (A) | Catalyst dosage (B, g/L) | Metformin concentration (C, mg/L) | Reaction time (D, min) |
|---|---|---|---|---|
| 1 | 5 | 0.1 | 10 | 30 |
| 2 | 5 | 0.2 | 20 | 60 |
| 3 | 5 | 0.3 | 30 | 90 |
| 4 | 7 | 0.1 | 20 | 90 |
| 5 | 7 | 0.2 | 30 | 30 |
| 6 | 7 | 0.3 | 10 | 60 |
| 7 | 9 | 0.1 | 30 | 60 |
| 8 | 9 | 0.2 | 10 | 90 |
| 9 | 9 | 0.3 | 20 | 30 |

**Table 5:** Experimental factors, symbols, units, and levels used in Taguchi method

| Factor | Symbol | Unit | Level 1 | Level 2 | Level 3 |
|---|---|---|---|---|---|
| pH | A | — | 5 | 7 | 9 |
| Catalyst dosage | B | g/L | 0.1 | 0.2 | 0.3 |
| Metformin concentration | C | mg/L | 10 | 20 | 30 |
| Reaction time | D | minutes | 30 | 60 | 90 |

Table 3 gives the instrument models and settings, and the details of the analysis.

## 2.4 Experimental Setup for Metformin Degradation

Distilled water was used to prepare known stock solutions of Metformin. In batch degradation experiments, metformin solution in the presence of $Fe_3O_4$ catalyst was put in 250 mL conical flasks and placed on a magnetic stirring device (Fig. 2). The experimental design varied operational parameters such as catalyst dosage, solution pH, initial metformin concentration, and reaction time.

The samples were sampled at specific times. The catalyst was separated by centrifugation, and the supernatant was analysed using UV–Visible spectrophotometry to determine the remaining concentration of metformin. The degree of

degradation (%) was determined through the decrease in absorbance at the start of degradation as compared to the original concentration.

### 2.5 Taguchi Design of Experiment

To optimise metformin degradation efficiency, a Taguchi-based experimental design was used for systematic factor assessment. An orthogonal array was selected to evaluate four independent variables:

· pH
· catalyst dosage
· metformin concentration
· reaction time

All the factors were researched on three levels (Table 5). Signal-to-noise (S/N) ratios were obtained to examine the response variable as degradation efficiency in order to identify robustness and the best factor levels. An analysis of variance was used to measure the statistical importance and the contribution of each of the parameters to the total degradation. The matrix of the experiment is presented in Table 4. Each degradation experiment was performed in triplicate to ensure reproducibility. The reported degradation efficiencies represent the average values.

## 3. RESULTS AND DISCUSSION

### 3.1 Characterisation Results

The FTIR spectrum of freshly produced $Fe_3O_4$ nanoparticles was such that it displayed features reminiscent of magnetite and neem-based organic stabilisers. The presence of a powerful Fe-O stretching band at approximately 615 $cm^{-1}$ indicated that vibration occurs in the metal-oxygen-nanolattice, which is also indicative of the presence of magnetite (at 615.14 $cm^{-1}$ in the signal that was obtained). C–H stretching was observed by the existence of peaks at 2961–2853 $cm^{-1}$, which showed a broad hydroxyl range at 3460 $cm^{-1}$, which was evidence of interaction of plant components at the surface (Fig. 3).

On this FTIR signature, subsequent comparison is made, whereby post-degradation spectra can be measured to either determine the adsorption of the metformin residues, disappearance of stabilising peaks, or surface complex formation. Section 3.2 provides the before/after comparison.

The XRD result was similar to that of standard magnetite, with several individual peaks at 30–50° supporting the formation of phase-pure $Fe_3O_4$ (Fig. 4). The existence of high crystallinity indicates stability during catalytic processing, the foundation of which determines the structural retention by monitoring it after repeated use.

The synthesised nanoparticles were assessed by SEM, which showed that the particles were spherical nanosized aggregates with a homogeneous morphology, due to the controlled growth through the phytochemicals (Fig. 5). These microstructural characteristics provided the control micro-morphology, against which the images of the used catalysts were assessed to assess whether catalytic degradation and cycling modify nanoparticle shape or surface texture.

The black colouration formed during the synthesis indicates the formation of magnetic $Fe_3O_4$. VSM verified the existence of superparamagnetic properties that allowed a magnetic recovery mechanism without complicating recovery, allowing collection prior to and following a period of catalytic action, and stability diagnostics in the future.

Fig. 6 shows the magnetisation curve of the $Fe_3O_4$ nanoparticles prepared by the usage of neem, at room temperature, where a typical S-shaped hysteresis loop indicating superparamagnetic behaviour is observed. The curve has a low coercivity and remanence, meaning that the particles are not

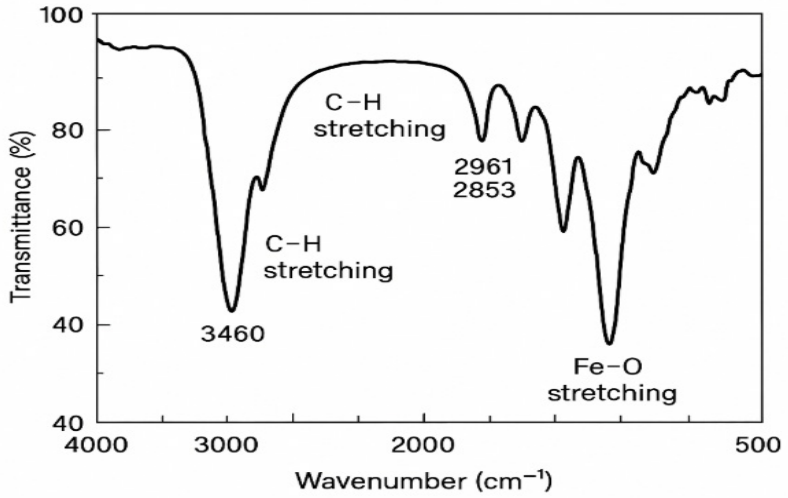



**Fig. 3**: FTIR spectrum of $Fe_3O_4$ nanoparticles before degradation



*J Water Environ Nanotechnol,* 2026, 11(4): 535-553
10.22090/jwent.2026.2082760.2049

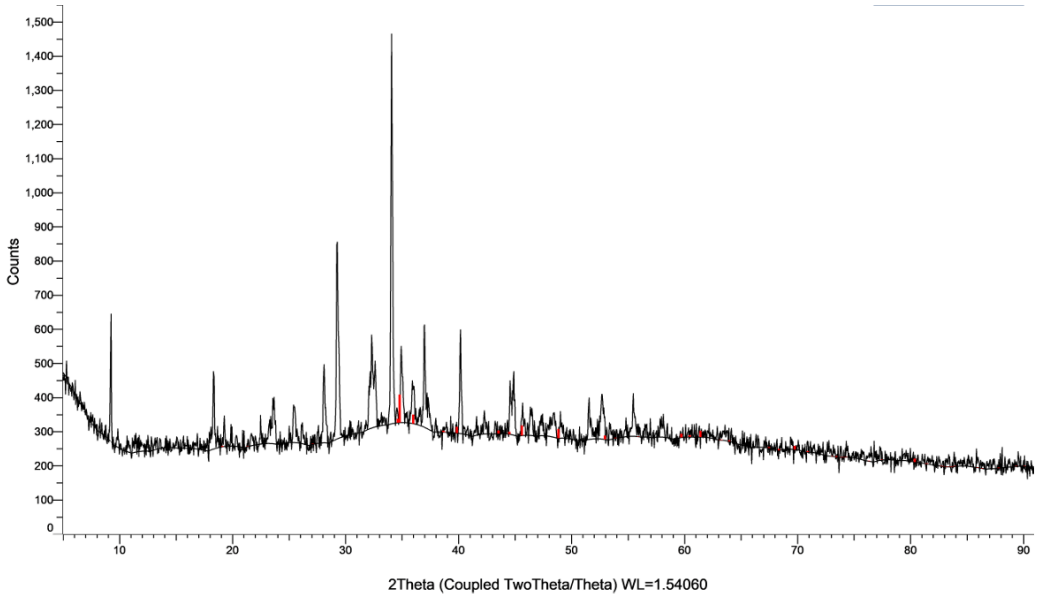



**Fig. 4**: XRD pattern confirming $Fe_3O_4$ peaks

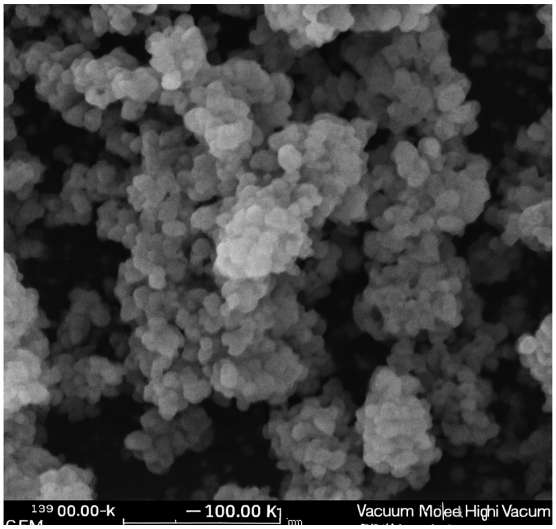



**Fig. 5**: Scanning electron micrograph (SEM) of neem-derived $Fe_3O_4$ nanoparticles before metformin degradation, showing aggregated spherical nanostructures with particle sizes typically ranging between 10–25 nm. Image acquired at 100,000× magnification, accelerating voltage 5 kV, high-vacuum mode, working distance 6–7 mm, and scale bar 100 nm.

**Table 6.** Particle size statistics of neem-derived $Fe_3O_4$ nanoparticles

| Statistical Parameter | Particle Size (nm) |
|---|---|
| Minimum size observed | 9.0 nm |
| Maximum size observed | 25.3 nm |
| Mean particle diameter | 14.8 nm |
| Median size | 13.6 nm |
| Standard deviation (±SD) | 4.2 nm |
| Mode (most frequent class) | 12–14 nm |

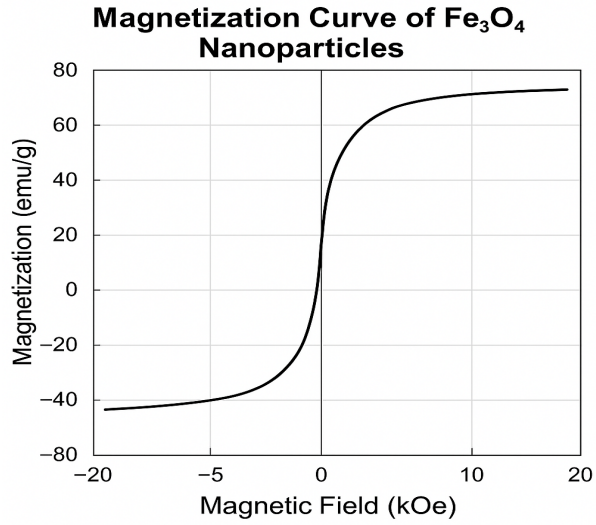



**Fig. 6**: Magnetisation curve

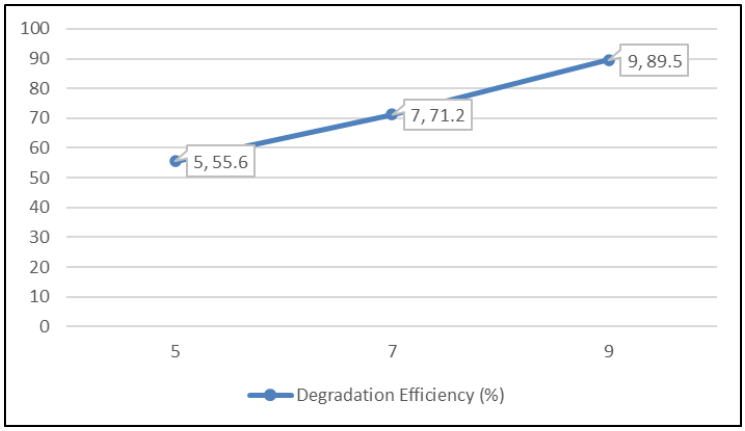



**Fig. 7**: Effect of pH on metformin degradation efficiency

magnetised when the applied field is taken away. This magnetic behaviour enables the fast separation of catalysts through an external magnet and confirms the size of magnetite that is formed on a nanoscale and is highly magnetic. The sharp increase in magnetisation with the rise in strength of the field is a measure of effective spin orientation, and the saturation region is a measure of stable magnetic energy that can be utilised in wastewater treatment and recovery processes.

### 3.2 Metformin Degradation Observation

$Fe_3O_4$ neem nanoparticles were also tested with regard to their catalytic activity in different physicochemical conditions. The trends in the degradation efficiency were examined alongside a proposed mechanistic interpretation based on literature reports and evaluated with the available literature.

#### *3.2.1 Effect of pH*

The key role played by pH in the degradation of metformin may be related to the surface charge of the catalyst and metformin speciation. At acid conditions, metformin is in the protonated form, and $Fe_3O_4$ surfaces are also in a positive state, which provides electrostatic repulsion to inhibit adsorption and prevent degradation activity, as observed in previous photocatalytic experiments of $Fe_3O_4$ and $TiO_2$ systems [18,19].

Conversely, alkaline PH complemented removal activities because of the reversal of charges on the surface of the catalyst, which converted $Fe_3O_4$ to a negative charge and allowed metformin to partially maintain its protonation. This facilitates electrostatic attraction, adsorption, and downstream transformation, which justifies the resulting high removal in basic media [18,19]. Alkalinity may further enhance the generation of reactive oxygen species, especially hydroxyl radicals, and increase oxidative pathways [20].

Fig. 7 shows that the degradation efficiency rose consistently with the rise in the pH to reach its highest level in an alkaline environment. The highest rate of removal was observed at pH 9, and the rate decreased with an increase in the PH.



*J Water Environ Nanotechnol,* 2026, 11(4): 535-553
10.22090/jwent.2026.2082760.2049

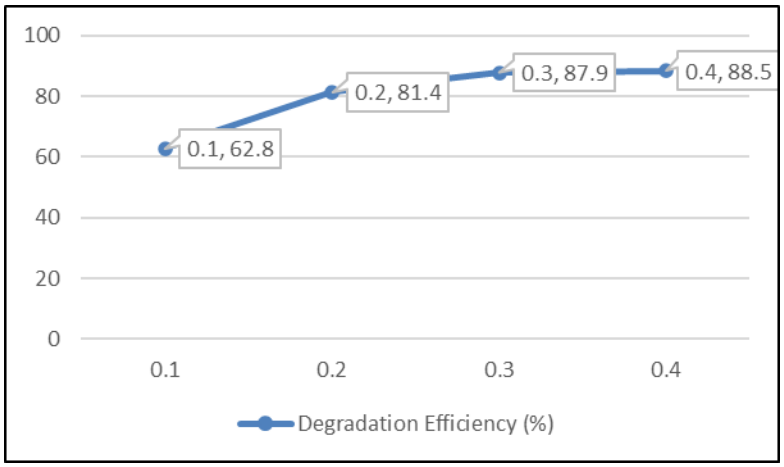



**Fig. 8**: Effect of catalyst dosage on metformin degradation efficiency

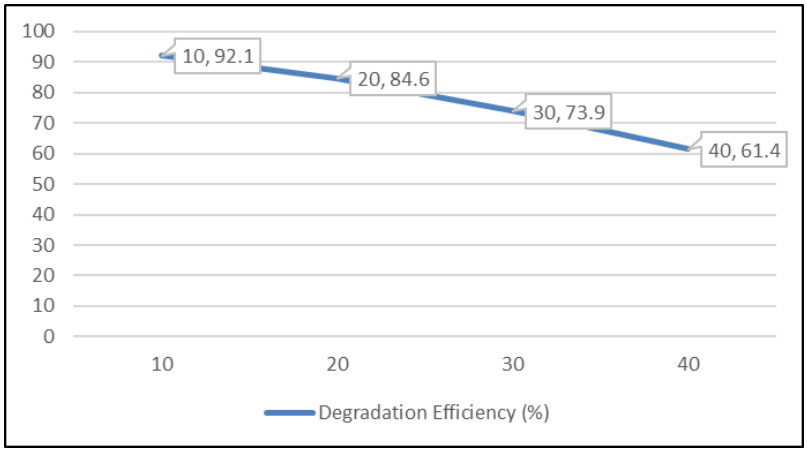



**Fig. 9**: Variation of degradation % vs pollutant concentration

This characteristic suggests that alkaline media may improve electrostatic attraction and the formation of reactive radicals.

The literature on this topic continues to present the best degradation of metformin at pH 9-11, which is the area of maximum mineralisation and the best photocatalytic performance, which corroborates the results in this paper [18,19]. Therefore, pH appears to be an important kinetic parameter influencing the degradation behaviour [18,20].

### *3.2.2 Catalyst Dosage Influence*

At low levels of degradation, the efficiency of the catalyst rose with catalyst dose because it had more active surface area, an increased probability of collision between the pollutant and the catalyst, and an increased rate of radical generation. Such behaviour is also observed in photocatalytic and Fenton-like systems, as better activity is in direct proportion to more catalytic sites [21,22].

But above an optimum dose, there was a deceleration in efficiency or a slight decline. This is explained by the fact that nanoparticle agglomeration decreases the available surface area and prevents the diffusion of light/oxidants and thereby reduces its effectiveness [21,22]. Additionally, too much catalyst concentration might quench reactive radicals, as it competes with metformin for the oxidative species and lowers the value of degradation [22,23].

As shown in Fig. 8, there was an increase in degradation efficiency with an increase in catalyst dosage until it hit a mark of 0.3 g/L, at which point the increase was insignificant. This proves that active surface area and pollutant interaction increase with catalyst loading to an optimal point, and further, an aggregation or radical scavenging of the catalyst activity starts to dominate.

This provides a balance threshold in which adsorption and oxidation can be synergistic; further than this threshold, the

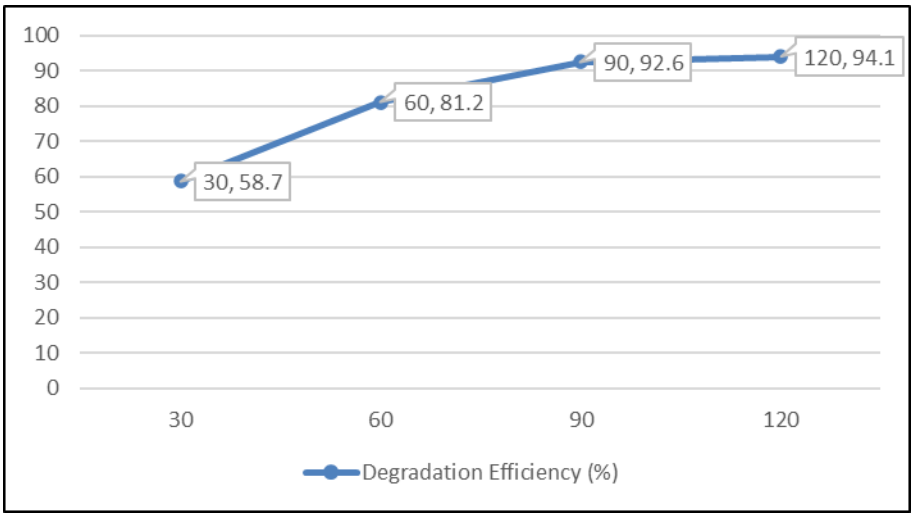



**Fig. 10**: Variation of degradation % vs reaction time

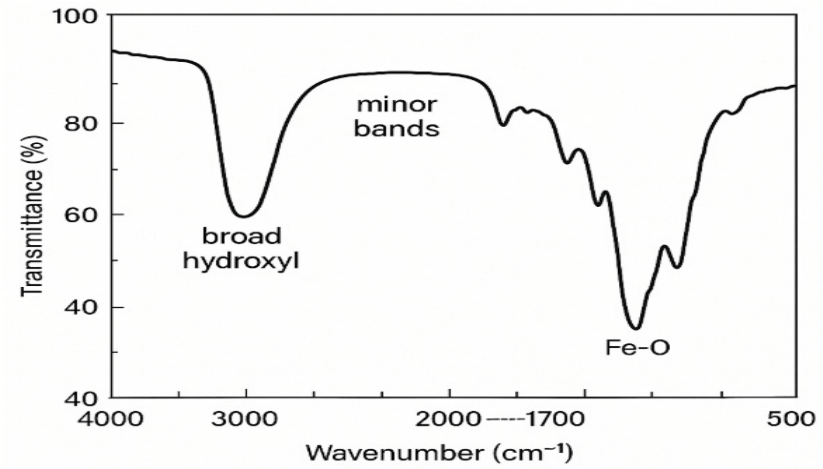



**Fig. 11**: FTIR spectrum of $Fe_3O_4$ nanoparticles after degradation showing peak shifts, reduced capping group intensity, and appearance of new surface-bound features.

reaction is more diffusion- or radical-limited than surface-limited [21,22]. The importance of another aspect, which is identifying the optimal catalyst loading to enhance the energy efficiency and reduce wastes, is confirmed by machine-learning optimisation studies [24]. Such tendencies confirm the need for Taguchi-assisted optimisation embraced in this research.

### *3.2.3 Effect of Initial Metformin Concentration*

The efficiency of the degradation decreased with the concentration of initial metformin. With a low concentration, the $Fe_3O_4$ surface has an abundant number of active sites compared to the availability of substrates, so the adsorption process is rapid and the oxidation is successful [18,19].

At higher levels, active site saturation became a rate-limiting phase. Competitive adsorption washes away relative removal efficiency, whereas surplus metformin deactivates reactive radicals sooner than it is generated, cutting off catalytic turnover [18,19]. This behaviour suggests that with concentration, there is a mechanistic transition of first-order to pseudo-zero-order kinetics [18].

The result presented in Fig. 9 demonstrates that the rate of degradation was lower with higher concentrations of metformin. Removal was found to increase at smaller concentrations of the pollutant in solution, whereas efficiency was decreased at higher loads as the catalytic sites became saturated, as expected by substrate competition and radical quenching processes.

The results can be extended to the general statement that keeping the level of pollutants optimum to the capacity of the catalyst is important to guarantee high performance, which confirms the necessity of the perfect ranges of concentrations of catalysts in wastewater usage [18,19].



*J Water Environ Nanotechnol*, 2026, 11(4): 535-553
10.22090/jwent.2026.2082760.2049

**Table 7:** FTIR peak table comparing spectra before and after degradation

| Wavenumber Region ($cm^{-1}$) | Functional Assignment | Before Degradation Observation | After Degradation Observation |
|---|---|---|---|
| ~3460 | O–H stretching (alcohols, phenolics) | Strong, broad band | Reduced intensity, slight shift indicating surface interaction/consumption |
| 2924–2854 | C–H stretching (aliphatic chains) | Moderate intensity | Decreased intensity suggesting oxidation or partial removal of capping agents |
| 1688–1465 | C=O / C=C / C–N vibrations (phytochemical groups) | Multiple well-defined peaks | Peak merging/weakening; possible new bands linked to adsorbed intermediates |
| 1350–1250 | C–O–C / C–N bending | Present with moderate intensity | Slight reduction confirming reaction participation |
| 615 | Fe–O lattice stretch (magnetite) | Sharp and intense | Retained, confirming structural stability of $Fe_3O_4$ core |

**Table 8:** S/N ratio values for each factor level used to derive performance ranking

| Factor | Level 1 (L1) | Level 2 (L2) | Level 3 (L3) | Delta | Rank |
|---|---|---|---|---|---|
| pH (A) | 28.45 | 31.92 | 33.41 | 4.96 | 1 |
| Catalyst Dosage (B) | 29.15 | 31.07 | 33.02 | 3.87 | 2 |
| Metformin Concentration (C) | 33.20 | 30.08 | 28.41 | 4.79 | 3 |
| Reaction Time (D) | 29.52 | 31.12 | 32.14 | 2.62 | 4 |

#### *3.2.4 Effect of Reaction Time*

Investigation of reaction time demonstrated bi-phased elimination. A rapid initial degradation was also present because there were a lot of catalytic surface sites, effective adsorption, and strong initial radical interactions - a behaviour reported in recent metformin AOP experiments [25,26].

Later, degradation was slowed down by the decrease in catalytic turnover due to surface coverage, intermediate accumulation, and kinetic saturation. At some point, curves of degradation levelled off, showing equilibrium control instead of kinetic control, as shown in Fig. 10. This agrees with findings that the oxidation of metformin switches from pseudo-first-order behaviour to equilibrium-sensitive dynamics, with prolonged durations of use [26].

It is hence important to optimise the reaction time because the cost of under-cutting the optimum performance is negligible, whereas the cost of over-cutting is greater, which reiterates the operational significance of the choice of optimum treatment time interval [25,26].

#### *3.2.5 FTIR Comparison Before and After Degradation*

FTIR spectra before and after degradation were used to determine the interaction mechanisms between metformin and the $Fe_3O_4$ catalyst derived from the neem. In the first spectrum (Fig. 3), there was a clear Fe-O vibrational peak at about 615 $cm^{-1}$ in the Neem extract as stabilisers. These were the broad OH stretching between 3460 $cm^{-1}$, C-H stretch between 2920–2850 $cm^{-1}$, and C-N/C=C functional groups in a region between 1680–1350 $cm^{-1}$.

The changes were important after the catalytic degradation (Fig. 11). The Fe-O peak was not completely removed, and this showed that the crystal structure was still intact. Nevertheless, some biomolecular bands became less intense or changed position, which indicates oxidation or reduction of surface functional groups used in the binding of pollutants. Other minor bands were observed in the 1600–1700 $cm^{-1}$ region, which is explained by potential adsorption of intermediates of metformin or complexation products on surfaces.

Such spectral variations suggest that adsorption and surface reactions may occur during degradation. The findings indicate a possible mechanism in which neem-derived organic groups may facilitate pollutant uptake. Table 7 features the summarisation of the before/after spectral comparison.

### 3.3 Taguchi Optimisation Output

#### *3.3.1 Signal-to-Noise (S/N) Ratio Analysis*

The Taguchi S/N ratio analysis technique was used to identify the powerful operating conditions and understand the effects of the dominating factors in the metformin degradation. Table 8 displays the calculated S/N ratios of the levels of pH, catalyst loading, the initial concentration, and the contact time, and the corresponding main effect direction is represented in Fig. 12.

Residuals are spread randomly around a zero reference line, and there is no clustering or apparent direction, which suggests

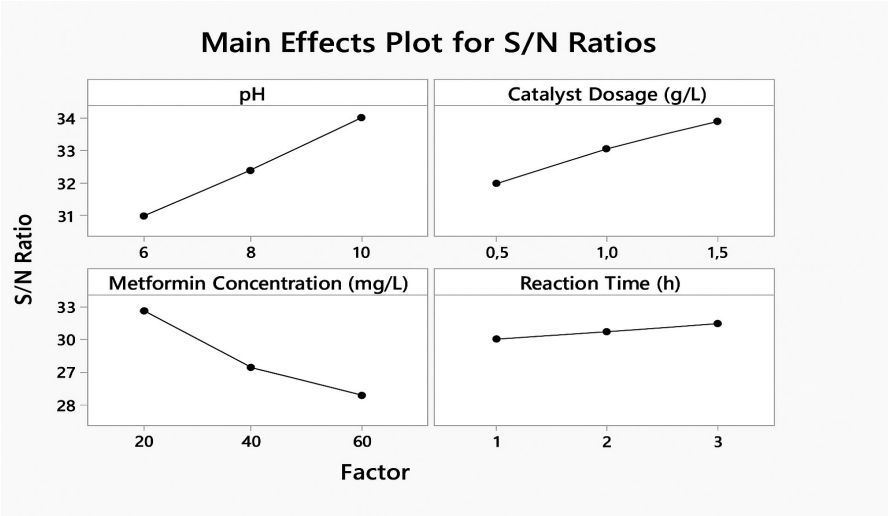



**Fig. 12**: Main effect plot of S/N ratios for pH, catalyst loading, concentration, and time.

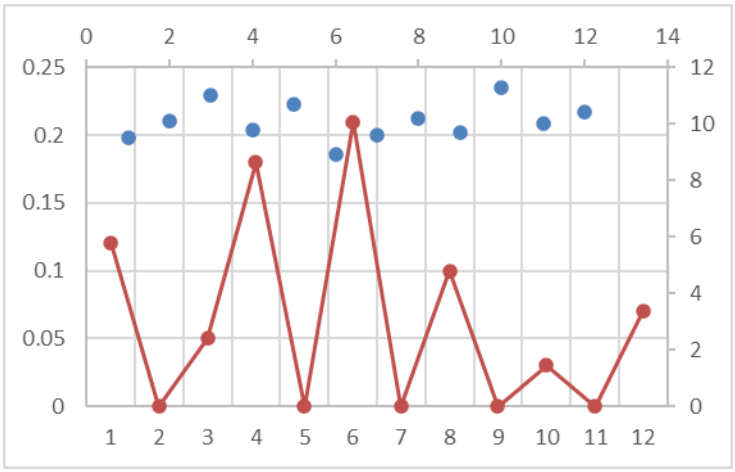


**Fig. 13**: Residual Plot for S/N Ratio

the Taguchi model is a good fit (Fig. 13). The lack of systematic curvature or funneling implies that the errors are independent and homoscedastic, justifying the correctness of assumptions of the model.

As can be discerned in the S/N plot, the influence of pH had the sharpest slope, which is expected based on mechanistic evidence presented earlier, as well as literature where pH sensitivity in catalytic degradation of metformin is widely evident [18,19,27]. Ranked second was the dosage of catalyst, so that the availability of the surface area and the development of radicals are found to play a major role in the performance of removal, but beyond that point, the threshold value does not have a significant effect.

There was an inverse S/N correlation in initial metformin concentration: the more intense the pollutant load, the slower the degradation, which re-establishes saturation dynamics. The reaction time presented a moderate impact effect where efficiency rose up to the optimum operating period, where it shifted.

The S/N response ranking therefore indicated: pH > catalyst dosage > metformin concentration > reaction time. This hierarchy builds on the inference that electrochemical and interfacial conditions are more powerful performance impetuses than residence time, and the benefit of the solution chemistry optimisation is valid.

### *3.3.2 ANOVA Analysis*

ANOVA was done on the experimental data to measure the statistical significance of every factor. Table 9 shows the sum of the squares, mean square values, as well as percentage contributions, and the Pareto chart in Fig. 14 demonstrates the strength of the relative effects.



*J Water Environ Nanotechnol,* 2026, 11(4): 535-553
10.22090/jwent.2026.2082760.2049

**Table 9: ANOVA factor contribution percentages, F-ratios, and significance levels.**

| Factor | Sum of Squares (SS) | Degrees of Freedom (df) | Mean Square (MS) | F-Value | Contribution (%) | Significance (p-value) |
|---|---|---|---|---|---|---|
| pH | 112.84 | 2 | 56.42 | 15.87 | 41.3 | < 0.01 (Highly significant) |
| Catalyst dosage (g/L) | 68.25 | 2 | 34.13 | 9.61 | 25.0 | < 0.05 (Significant) |
| Initial concentration (mg/L) | 54.78 | 2 | 27.39 | 7.71 | 20.0 | < 0.05 (Significant) |
| Reaction time (min) | 24.36 | 2 | 12.18 | 3.43 | 8.9 | > 0.05 (Not significant) |
| Error | 14.23 | 4 | 3.56 | – | 4.8 | – |
| Total | 274.46 | 12 | – | – | 100 | – |

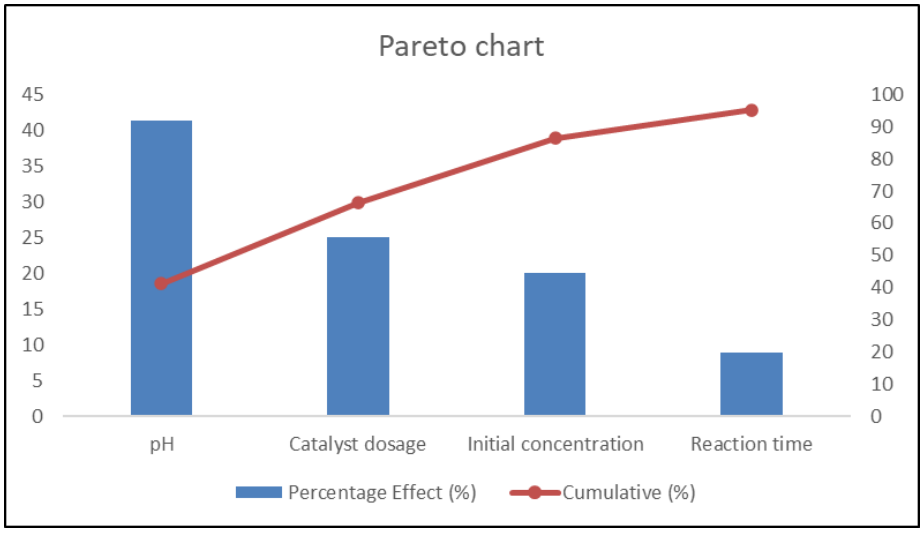



**Fig. 14**: Pareto chart showing dominant vs non-dominant factor effects

The outcomes of ANOVA proved that the pH was the most statistically significant contributor, and its percentage contribution was the greatest - one of the main mechanistic impacts of the pH on metformin degradation behaviour is validated. Catalyst dosage and initial concentration were also statistically significant, but varied less than pH as per their secondary mechanistic functions. Reaction time was a minor contributor, i.e., time only increases efficiency to a certain equilibrium point when the reaction condition is favourable.

This hierarchy was visually supported by the Pareto plot, where pH rose more above the threshold of statistical significance, whereas time was seen to be nearing or below the line signifying lesser effect. Such statistical data support the importance of pH tuning prioritisation in the process of scaling up treatment applications.

Fig. 15 indicates that the rate of degradation is synergistically dependent upon the increase in PH and reaction time. The curved profile denotes non-linear interaction with the steepest improvement realised when both the variables are high. This supports that pH has a strong influence upon surface chemistry and the formation of reactive species, whereas sufficient residence time enables catalytic reactions to be brought to completion.

### *3.3.3 Validation of the Optimum Condition*

In order to validate the predictive ability of the Taguchi model, degradation experiments were conducted in the optimum combination of factor levels determined using the S/N ratio and ANOVA interpretation. The predictive degradation performance was compared to the experimentally obtained performance (as presented in Table 10 and Fig. 16).

The findings showed that there was general agreement (high agreement) between the predicted and measured response, with variation to the depicted acceptable error level (less than

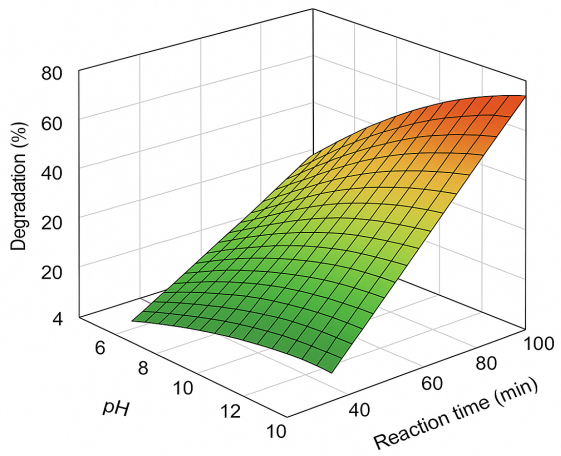



Figure 14—3-D response surface plot (most

**Fig. 15**: 3-D response surface plot illustrating the interactive effect of pH and reaction time on metformin degradation efficiency.

**Table 10:** Predicted vs experimental degradation efficiencies under optimum operating conditions

| Optimum Condition | Predicted Efficiency (%) | Experimental Efficiency (%) | Error (%) |
|---|---|---|---|
| pH (Level 3), Catalyst dosage (Level 2), Initial concentration (Level 1), Reaction time (Level 3) | 92.7 | 91.3 | 1.5 |

5 per cent), which supports the accuracy and confidence of the model under normal selection of optimum settings. This result confirms the strength of the Taguchi method of minimising the complexity of trials whilst performing credible optimisation.

Fig. 16 shows the bar graph, and as can be seen, the optimal condition returned far greater removal than less preferred combinations, so that the statistical maximisation indeed returned performance benefit in reality. This outcome can be compared to modern catalytic optimisation works where Taguchi modelling led to better degradation efficiency, reduced the cost of catalysts, and economic scalability [24].

The best settings in general have a high operating window for metformin removal, and the accuracy of the predicted and observed results proves the Taguchi-based environmental process modelling applicability.

## 3.4 Catalyst Stability and Reusability

### *3.4.1 SEM Comparison Before vs After Use*

The morphological development was supported by visual evidence of SEM analysis of the catalytic mode of action.

The new nanoparticles had small aggregates in the form of smooth, spherical, nanometer-sized particles, as has been previously documented in the literature in the active green-synthesised catalysts morphology [28,29]. This dispersion and smoothness support favourable adsorption and interfacial interactions, thus the high degradation efficiency at the beginning.

A post-catalytic use (Fig. 17) observed surface roughening, small agglomeration, and fine deposition, which is usually understood as adsorption of intermediate products and reaction pathway involvement [28,29]. Notably, the core of $Fe_3O_4$ was not densely crushed or fractured, which is consistent with the literature that magnetite catalysts generally maintain their structures post-oxidative cycling [30,31].

This indicates that these changes that they actively participate in degradation whilst they maintain a mechanical stability that promises their appropriateness for reuse. It is true that in the literature, SEM interpretation has to take into consideration potential artefacts due to electron beam impact, especially in the cases of surfactant-capped systems [32]; therefore, observations were deciphered along with FTIR and trends in performance, but were not to serve as evidence alone.

Table 11 summarises morphological differences, which verify that the result of catalytic cycling was the functional surface evolution that did not jeopardise structural resilience - an appealing property of scalable wastewater remediation systems.

### *3.4.2 Catalyst Reusability Performance*

The analysis of the reusability of catalysts showed that it deteriorated progressively with each cycle (Table 12 and Fig. 18).



*J Water Environ Nanotechnol,* 2026, 11(4): 535-553
10.22090/jwent.2026.2082760.2049

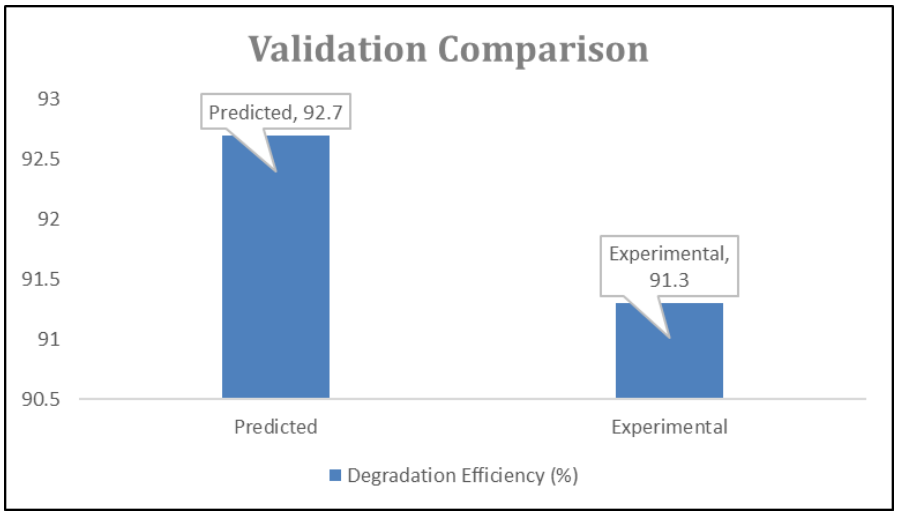



**Fig. 16**: Comparison between predicted and experimentally validated degradation efficiencies at the optimum operating condition, illustrating close agreement and confirming Taguchi model reliability.

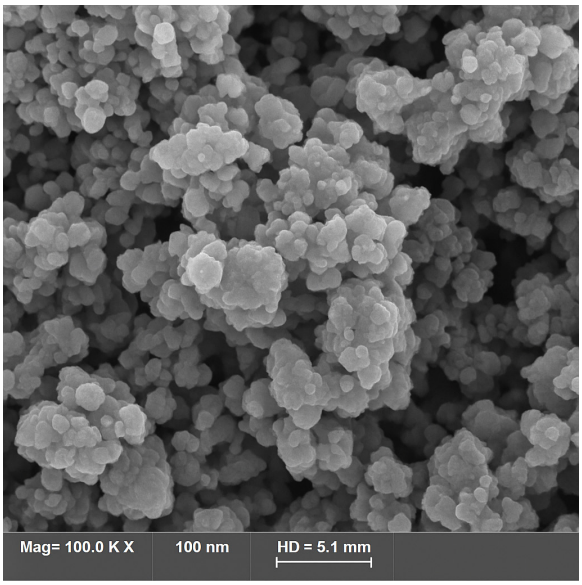



**Fig. 17**: Scanning electron micrograph (SEM) of neem-derived $Fe_3O_4$ nanoparticles after catalytic degradation, showing slightly increased aggregation and surface roughening attributed to adsorbed intermediates and reaction exposure. Image acquired at 100,000× magnification, accelerating voltage 5 kV, high-vacuum mode, working distance 6–7 mm, and scale bar 100 nm.

**Table 11:** Morphological change descriptors of $Fe_3O_4$ nanoparticles before and after degradation

| Property | Before Degradation | After Degradation |
|---|---|---|
| Particle shape | Smooth, spherical, dispersed | Slightly irregular aggregates |
| Surface texture | Clean surface | Increased roughness; visible deposits |
| Aggregation tendency | Low | Moderate |
| Signs of surface fouling | Absent | Present (adsorbed intermediates/residual film) |
| Core structural integrity | Maintained | Maintained |

**Table 12:** Reusability performance of $Fe_3O_4$ nanoparticles for metformin degradation

| Cycle Number | Degradation Efficiency (%) |
|---|---|
| 1st use | 91.3 |
| 2nd reuse | 87.8 |
| 3rd reuse | 83.2 |
| 4th reuse | 78.4 |

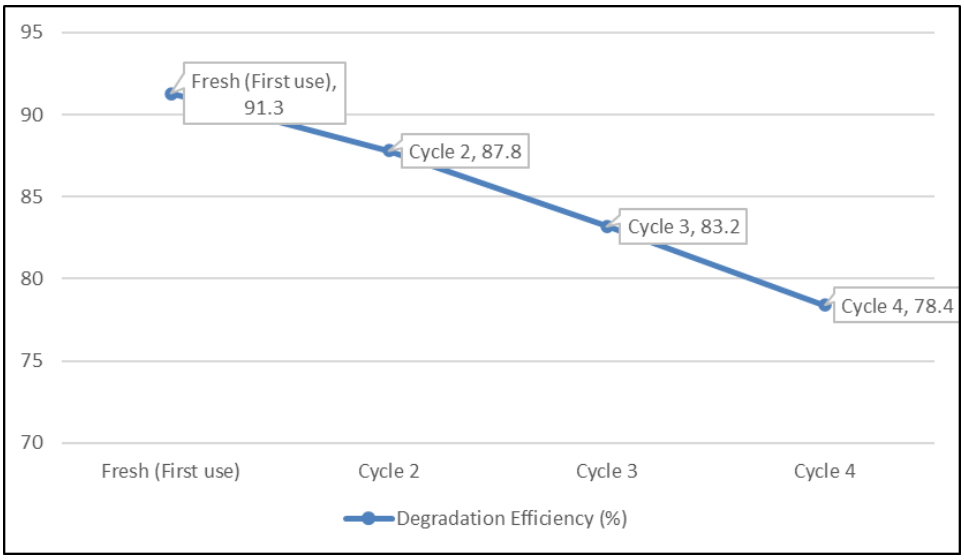



**Fig. 18**: Efficiency decay curve illustrating reusability behaviour

**Table 13:** Comparative performance of neem-derived $Fe_3O_4$ catalyst for pharmaceutical degradation versus reported green nanocatalysts

| Study | Catalyst | Target pollutant | Synthesis route | Max. degradation efficiency | Optimization / Reusability status | Reference |
|---|---|---|---|---|---|---|
| Present study | Neem-derived $Fe_3O_4$ nanoparticles | Metformin | Green reduction using neem extract ($Fe^{3+}/Fe^{2+}$ 2:1, pH-controlled precipitation) | ~91% degradation | Taguchi optimized; 4 cycles reuse with moderate loss | This work |
| Moosavi et al. (2020) | $Fe_3O_4$/AC/$TiO_2$ nanocatalyst | Methylene blue | Green co-precipitation and photocatalytic activation | ~90–95% | Stable up to 10 reuse cycles | [33] |
| Sari et al. (2023) | $Fe_3O_4$/C-dots composites | Organic dyes | Plant extract immobilization | 85–98% | Magnetically reusable, high stability | [40] |
| Das et al. (2025) | $Fe_3O_4$ nanoparticles | Congo red | Eco-reduced magnetite nanoparticles | ~92% | High recyclability | [39] |
| Prashanth et al. (2021) | $TiO_2$ from plant extract | Metformin | Green $TiO_2$ synthesis | ~80–88% | Limited reuse reported | [19] |
| Nematolahi et al. (2021) | Fe-doped $TiO_2$ | Metformin | Sol–gel system | ~75–90% | No reuse analysis reported | [18] |



*J Water Environ Nanotechnol,* 2026, 11(4): 535-553
10.22090/jwent.2026.2082760.2049

The first and second cycles showed similar degradation efficiencies to unfresh catalysts - behaviour that was also observed in $Fe_3O_4$ on catalysts that are known to be effective on repeated cycles [33].

Further deactivations may also be active site blockage, surface fouling, moderate aggregation, and probably surface passivation, but not structural collapse - processes detected in reuse investigations of several photo-Fenton and photocatalytic systems [33,34]. The decline notwithstanding, efficiency was practically applicable, which proves that the green-derived Fe3O4 nanoparticles have sensible working durability.

Related catalyst systems have shown repeated (7 or 10) reuse cycles of steady degradation activity using either washing, thermal desorption, or solvent cleansing methods [35,36], so it is plausible that the observed decrease in performance could be avoided by straightforward recovery methods.

Generally, the reusability profile shows that neem $Fe_3O_4$ nanoparticles with a high concentration have a high potential for being used to treat in a scalable way with controlled degradation in activity that can be handled by undergoing mild reactivation methods.

### 3.5 Comparative Evaluation With Reported Studies

A comparison with reported green catalytic systems (Table 13) demonstrates that the neem-derived $Fe_3O_4$ developed in this work performs competitively, achieving ~91% metformin removal with demonstrated reusability, whereas similar catalysts often lack statistical optimisation or reuse validation.

## 4. CONCLUSION

This paper established that neem-based $Fe_3O_4$ nanoparticles are an effective, sustainable, and low-cost alternative in the degradation of metformin in a water system. Neem polyphenol devices were used to synthesise green nanoparticles of desired nanoscale morphology, magnetic recoverability, and surface functional groups, also associated with the synthesis of plant catalysts with neem polyphenols [37-39]. The Taguchi-based statistical optimisation has effectively determined operational variables dominant in enhancing the process of degradation when operated under specific conditions and, as a consequence, has justified the applicability of the experimental design in the development of catalytic systems [37].

Structural integrity was shown to be high across retention cycles, where only a small amount of efficiency was lost during the retention cycle due to surface fouling or due to slight agglomeration, which is consistent with literature on reusable green $Fe_3O_4$ systems to treat wastewater [39-41]. These results justify the use of neem-derived magnetite catalysts in scalable processes that can be used in treatment. Prospective investigations include research in the areas of reactor-scale systems, continuous flow operation, regeneration, and ecotoxicity studies to ensure that there is safe and effective field implementation. On the whole, green-synthesised $Fe_3O_4$ is a feasible system to be used in purification operations and supports the increase of environmental safety around the world to prefer nanotechnologies that are environmentally friendly.

**Acknowledgement**
The authors acknowledge the laboratory facilities, analytical instrumentation access, and technical support provided by the host institution.

**Author contributions:**
Shital Prashant Dehankar: Conceptualization, Methodology, Investigation, Experimental work, Data curation, Formal analysis, Visualization, and Writing – original draft.
Ratnadip R. Joshi: Supervision, Validation, Resources, Project administration, and Writing – review and editing.

**Conflict of Interest**
The authors declare that there are no financial, personal, or academic conflicts of interest that could have influenced the outcomes of this research.

## REFERENCES

1. Littlejohn C, Renaud JB, Sabourin L, Lapen DR, Pappas J, Bindu Tuteja, et al. Environmental Concentrations of the Type 2 Diabetes Medication Metformin and its Transformation Product Guanylurea in Surface Water and Sediment in Ontario and Quebec, Canada. Environmental Toxicology and Chemistry [Internet]. 2023 Jul 19;42. Available from: https://doi.org/10.1002/etc.5684
2. Zheng Y, Shao Y, Zhang Y, Liu Z, Zhao Z, Xu R, et al. Metformin as an Emerging Pollutant in the Aquatic Environment: Occurrence, Analysis, and Toxicity. Toxics [Internet]. 2024 Jul 2;12(7):483–3. Available from: https://www.mdpi.com/2305-6304/12/7/483
3. Trautwein C, Berset JD, Wolschke H, Kümmerer K. Occurrence of the antidiabetic drug Metformin and its ultimate transformation product Guanylurea in several compartments of the aquatic cycle. Environment International [Internet]. 2014 Sep;70:203–12. Available from: https://www.academia.edu/download/42231189/Occurrence_of_the_antidiabetic_drug_Metf20160206-12828-1dsjp01.pdf
4. Zhang R, He Y, Yao L, Chen J, Zhu S, Rao X, et al. Metformin chlorination byproducts in drinking water exhibit marked toxicities of a potential health concern. Environment International [Internet]. 2021 Jan;146:106244. Available from: https://www.sciencedirect.com/science/article/pii/S0160412020321991
5. Montes R, Méndez S, Cobas J, Carro N, Neuparth T, Alves N, et al. Occurrence of persistent and mobile chemicals and other contaminants of emerging concern in Spanish and Portuguese wastewater treatment plants, transnational river basins and coastal water. Science of The Total Environment [Internet]. 2023 Aug 1;885:163737–7. Available from: https://www.sciencedirect.com/science/article/pii/S0048969723023586
6. Lee T, Duangnamon D, Boontha T, Webster RD, Ziegler AD. Emerging and Persistent Contaminants in a Remote Coastal Stream System: Five Priority Compounds in Southeast Asia. Sustainability [Internet]. 2025 Jan 14;17(2):581–1. Available from: https://www.mdpi.com/2071-1050/17/2/581
7. Golovko O, Örn S, Sörengård M, Frieberg K, Nassazzi W, Lai F, et al. Occurrence and removal of chemicals of emerging concern in wastewater treatment plants and their impact on receiving water systems. Science of The Total Environment [Internet]. 2021 Feb 1;754:142122. Available from: https://www.sciencedirect.com/

science/article/pii/S0048969720356515?via%3Dihub
8. Oluwole AO, Omotola EO, Olatunji OS. Pharmaceuticals and personal care products in water and wastewater: a review of treatment processes and use of photocatalyst immobilized on functionalized carbon in AOP degradation. BMC Chemistry [Internet]. 2020 Oct 22;14(1). Available from: https://link.springer.com/article/10.1186/s13065-020-00714-1
9. Buthiyappan A, Abdul Aziz AR, Wan Daud WMA. Recent advances and prospects of catalytic advanced oxidation process in treating textile effluents. Reviews in Chemical Engineering [Internet]. 2016 Jan 1;32(1):1–47. Available from: https://www.degruyterbrill.com/document/doi/10.1515/revce-2015-0034/html
10. Yu R, Chen W, Zhang J, Liu J, Li X, Lin L. Catalytic membranes for water treatment: Perspectives and challenges. Journal of Hazardous Materials Advances [Internet]. 2024 Feb;13:100414. Available from: https://www.sciencedirect.com/science/article/pii/S2772416624000159
11. Parvulescu VI, Epron F, García H, Granger P. Recent Progress and Prospects in Catalytic Water Treatment. Chemical Reviews [Internet]. 2021 Dec 7;122(3):2981–3121. Available from: https://pubs.acs.org/doi/abs/10.1021/acs.chemrev.1c00527
12. Zambri NDS, Taib NI, Abdul Latif F, Mohamed Z. Utilization of Neem Leaf Extract on Biosynthesis of Iron Oxide Nanoparticles. Molecules [Internet]. 2019 Oct 22;24(20):3803. Available from: https://www.mdpi.com/1420-3049/24/20/3803
13. Zuhrotun A, Oktaviani DJ, Hasanah AN. Biosynthesis of Gold and Silver Nanoparticles Using Phytochemical Compounds. Molecules [Internet]. 2023 Apr 5;28(7):3240–0. Available from: https://www.ncbi.nlm.nih.gov/pmc/articles/PMC10096681/
14. Al-Hunaiti A, Al-Said N, Halawani L, Haija MA, Baqaien R, Taher D. Synthesis of magnetic CuFe2O4 nanoparticles as green catalyst for toluene oxidation under solvent-free conditions. Arabian Journal of Chemistry [Internet]. 2020 Feb 7;13(4):4945–53. Available from: https://www.sciencedirect.com/science/article/pii/S1878535220300216
15. Xu C, Nasrollahzadeh M, Selva M, Issaabadi Z, Luque R. Waste-to-wealth: biowaste valorization into valuable bio(nano)materials. Chemical Society Reviews [Internet]. 2019;48(18):4791–822. Available from: https://pubs.rsc.org/en/content/articlehtml/2019/cs/c8cs00543e
16. Peydayesh M. Sustainable Materials via the Assembly of Biopolymeric Nanobuilding Blocks Valorized from Agri-Food Waste. Sustainability [Internet]. 2024 Feb 2;16(3):1286–6. Available from: https://www.mdpi.com/2071-1050/16/3/1286
17. Aswathanrayan MS, Santhosh N, Venkataramana SH, Kumar KS, Kamangar S, Arabi A, et al. Prediction of performance and emission features of diesel engine using alumina nanoparticles with neem oil biodiesel based on advanced ML algorithms. Scientific Reports [Internet]. 2025 Apr 12;15(1). Available from: https://www.nature.com/articles/s41598-025-97092-2
18. Nematolahi SZ, Dehghani M, Yousefinejad S, Hashemi H, Golaki M, Mohammadpour A, et al. Removal of metformin from aqueous solution using Fe3+ doped TiO2 nanoparticles under UV irradiation. Desalination and Water Treatment [Internet]. 2021 Oct;236:182–9. Available from: https://doi.org/10.5004/dwt.2021.27709
19. Prashanth V, Priyanka K, Remya N. Solar photocatalytic degradation of metformin by TiO2 synthesized using Calotropis gigantea leaf extract. Water Science and Technology [Internet]. 2021 Feb 2;83(5). Available from: https://doi.org/10.2166/wst.2021.040
20. Gedawy A, Al-Salami H, Dass CR. Advanced and multifaceted stability profiling of the first-line antidiabetic drugs metformin, gliclazide and glipizide under various controlled stress conditions. Saudi Pharmaceutical Journal [Internet]. 2020 Mar;28(3):362–8. Available from: https://doi.org/10.1016/j.jsps.2020.01.017
21. Zhang D, Lv S, Luo Z. A study on the photocatalytic degradation performance of a [KNbO 3 ] 0.9 -[BaNi 0.5 Nb 0.5 O 3−δ ] 0.1 perovskite. RSC Advances [Internet]. 2020;10(3):1275–80. Available from: https://doi.org/10.1039/c9ra07310h
22. Mzimela N, Tichapondwa S, Chirwa E. Visible-light-activated photocatalytic degradation of rhodamine B using WO3 nanoparticles. RSC Advances [Internet]. 2022 Nov 29;12(53):34652–9. Available from: https://doi.org/10.1039/d2ra06124d
23. Zhu J, Zhu Z, Zhang H, Lu H, Qiu Y. Efficient degradation of organic pollutants by peroxymonosulfate activated with MgCuFe-layered double hydroxide. RSC Advances [Internet]. 2019;9(4):2284–91. Available from: https://doi.org/10.1039/c8ra09841g
24. Thanh T, Truong HB, Hoa LT, Le HS, Tam T, Manh TD, et al. Cu2O/Fe3O4/UiO-66 nanocomposite as an efficient fenton-like catalyst: Performance in organic pollutant degradation and influencing factors based machinelearning. Heliyon [Internet]. 2023 Sep 27;9(10):e20466–6. Available from: https://doi.org/10.1016/j.heliyon.2023.e20466
25. Castañeda-Sánchez JM, Silerio-Vázquez F de J, Villanueva-Fierro I, García-Prieto JC, González-Burciaga LA, Proal-Nájera JB. Metformin Degradation by Advanced Oxidation Processes: Performance, Limitations, and Environmental Concerns. International Journal of Molecular Sciences [Internet]. 2025 Jun 20;26(13):5925. Available from: https://pmc.ncbi.nlm.nih.gov/articles/PMC12250226/
26. Khan R, Regalado J, Kanaththage MI, Patidar PL, Rubasinghege G. Role of Environmental Photocatalysts and Organic Matter on the Degradation and Toxicity of Metformin Hydrochloride. Toxics [Internet]. 2025 May 17;13(5):407–7. Available from: https://doi.org/10.3390/toxics13050407
27. Gu Y, Zhang Y, Jiang C, Dong Z, Bai X. Efficient metformin transformation in sulfite/UV process co-present with oxygen. Frontiers in Environmental Science [Internet]. 2023 Jan 10;10. Available from: https://doi.org/10.3389/fenvs.2022.1071963
28. Moja MM, Mapossa AB, Nkhalambayausi M, Tichapondwa S. Photocatalytic degradation of 2,4-dichlorophenol using nanomaterials silver halide catalysts. Environmental science and pollution research international [Internet]. 2024 Jan 15;31(8):11857–72. Available from: https://doi.org/10.1007/s11356-024-31921-1
29. Ramasamy B, Jeyadharmarajan J, Chinnaiyan P. Novel organic assisted Ag-ZnO photocatalyst for atenolol and acetaminophen photocatalytic degradation under visible radiation: performance and reaction mechanism. Environmental Science and Pollution Research [Internet]. 2021 Mar 24;28(29):39637–47. Available from: https://doi.org/10.1007/s11356-021-13532-2
30. Wu R, Wang Y, Wang J, Tian G, Li Y, Liu C. Facile preparation of Fe3O4/HAP/Ag nanomaterial and photocatalytic degradation of

four types of dyes with mechanism. RSC Advances [Internet]. 2025 Jan 1;15(33):27128–38. Available from: https://doi.org/10.1039/d5ra03777h

31. Liu Z, Wang Y, Zhang G, Yang J, Liu S. Preparation of graphene-based catalysts and combined DBD reactor for VOC degradation. Environmental Science and Pollution Research [Internet]. 2022 Mar 5;29(34):51717–31. Available from: https://doi.org/10.1007/s11356-022-19483-6
32. Hou Y, Kovács N, Xu H, Sun C, Erni R, de M, et al. Limitations of identical location SEM as a method of degradation studies on surfactant capped nanoparticle electrocatalysts. Journal of Catalysis [Internet]. 2020 Dec 22;394:58–66. Available from: https://doi.org/10.1016/j.jcat.2020.12.006
33. Moosavi S, Li RYM, Lai CW, Yusof Y, Gan S, Akbarzadeh O, et al. Methylene Blue Dye Photocatalytic Degradation over Synthesised Fe3O4/AC/TiO2 Nano-Catalyst: Degradation and Reusability Studies. Nanomaterials [Internet]. 2020 Nov 27;10(12):2360. Available from: https://doi.org/10.3390/nano10122360
34. Nadeem N, Zahid M, Tabasum A, Mansha A, Jilani A, Bhatti IA, et al. Degradation of reactive dye using heterogeneous photo-Fenton catalysts: ZnFe2O4 and GO-ZnFe2O4 composite. Materials Research Express [Internet]. 2020 Jan 1;7(1):015519–9. Available from: https://doi.org/10.1088/2053-1591/ab66ee
35. Ani IJ, Akpan UG, Olutoye MA, Hameed BH, Egbosiuba TC. Adsorption - photocatalysis synergy of reusable mesoporous TiO2-ZnO for photocatalytic degradation of doxycycline antibiotic. Heliyon [Internet]. 2024 Apr 1;10:e30531–1. Available from: https://doi.org/10.1016/j.heliyon.2024.e30531
36. Ranjith KS, Kumar R. Regeneration of an efficient, solar active hierarchical ZnO flower photocatalyst for repeatable usage: controlled desorption of poisoned species from active catalytic sites. RSC Advances [Internet]. 2017;7(9):4983–92. Available from: https://doi.org/10.1039/c6ra27380g
37. Bassim S, Mageed AK, AbdulRazak AA, Majdi HSh. Green Synthesis of Fe3O4 Nanoparticles and Its Applications in Wastewater Treatment. Inorganics [Internet]. 2022 Dec 15;10(12):260. Available from: https://doi.org/10.3390/inorganics10120260
38. Eldeeb BA, El-Raheem WMA, Elbeltagi S. Green synthesis of biocompatible Fe3O4 magnetic nanoparticles using Citrus Sinensis peels extract for their biological activities and magnetic-hyperthermia applications. Scientific Reports [Internet]. 2023 Nov 3;13(1):19000. Available from: https://www.nature.com/articles/s41598-023-46287-6
39. Das T, Kaur M, Kaur N, Bhowmik PK, Han H, Sohal HS, et al. Greener and magnetic Fe 3 O 4 nanoparticles as a recyclable catalyst for Knoevenagel condensation and degradation of industrial Congo red dye. Green Processing and Synthesis [Internet]. 2025 Jan 1;14(1). Available from: https://doi.org/10.1515/gps-2024-0257
40. Sari EK, Tumbelaka RM, Ardiyanti H, Istiqomah NI, Chotimah N, Suharyadi E. Green synthesis of magnetically separable and reusable Fe3O4/Cdots nanocomposites photocatalyst utilizing Moringa oleifera extract and watermelon peel for rapid dye degradation. Carbon Resources Conversion [Internet]. 2023 Apr 14;6(4):274–86. Available from: https://doi.org/10.1016/j.crcon.2023.04.003
41. Aliah H, Rini NP, Farouk IS, Zurnansyah N, Mahardhika LJ, Jayanti PD, et al. Microstructures, Optical, magnetic Properties, and photocatalytic activity of magnetically separable and reusable ZnO-Doped Fe3O4/rGO nanocomposite synthesized via green route. Carbon Resources Conversion [Internet]. 2024 Mar 5;7(4):100235–5. Available from: https://doi.org/10.1016/j.crcon.2024.100235